

PLASMIN POTENTIATES SYNAPTIC NMDA RECEPTOR FUNCTION IN HIPPOCAMPAL NEURONS THROUGH ACTIVATION OF PAR1

Guido Mannaioni¹, Anna G. Orr², Cecily E. Hamill², Hongjie Yuan², Katherine H. Pedone², Kelly L. McCoy², Rolando B. Palmieri¹, Candice E. Junge³, C. Justin Lee⁴, Manuel Yepes⁵, John R. Hepler², and Stephen F. Traynelis²

¹Dipartimento di Farmacologia, Università degli Studi di Firenze, Firenze, Italy

²Department of Pharmacology, Emory University School of Medicine, Atlanta, GA

³Agensys Inc., Santa Monica, CA 90404

⁴Korean Institute of Technology, Seoul, Korea

⁵Department of Neurology, Emory University School of Medicine, Atlanta, GA

Running head: Plasmin potentiates NMDA receptor function

Address correspondence to: Stephen F. Traynelis, PhD, Department of Pharmacology, 5062 Rollins Research Center, 1510 Clifton Road, Emory University, Atlanta, GA 30322. Tel: 404-727-0357; Fax: 404-313-0365; E-mail: strayne@emory.edu

Protease-activated receptor-1 (PAR1) is activated by a number of serine proteases, including plasmin. Both PAR1 and plasminogen, the precursor of plasmin, are expressed in the central nervous system. In this study, we examined the effects of plasmin in astrocyte and neuronal cultures as well as in hippocampal slices. We find that plasmin evokes an increase in both phosphoinositide hydrolysis (EC_{50} 64 nM) and Fura-2/AM fluorescence (195 ± 6.7 % above baseline, EC_{50} 65 nM) in cortical cultured murine astrocytes. Plasmin also activates extracellular signal-regulated kinase (ERK1/2) within cultured astrocytes. The plasmin-induced rise in intracellular Ca^{2+} concentration ($[Ca^{2+}]_i$), as well as the increase in phospho-ERK1/2 levels, was diminished in PAR1^{-/-} astrocytes and was blocked by 1 μ M BMS-200261, a selective PAR1 antagonist. However, plasmin had no detectable effect on ERK1/2 or $[Ca^{2+}]_i$ signaling in primary cultured hippocampal neurons or in CA1 pyramidal cells in hippocampal slices. Plasmin (100-200 nM) application potentiated the NMDA receptor-dependent component of miniature excitatory postsynaptic currents recorded from CA1 pyramidal neurons, but had no effect on AMPA or GABA receptor-mediated synaptic currents. Plasmin also increased NMDA-induced whole cell receptor currents recorded from CA1 pyramidal cells (2.5 ± 0.3 fold potentiation over control). This effect was blocked by BMS-200261 (1 μ M; 1.02 ± 0.09 fold potentiation over control). These data suggest that plasmin may serve as an endogenous PAR1 activator that can increase $[Ca^{2+}]_i$ in astrocytes and potentiate NMDA receptor synaptic currents in CA1 pyramidal neurons.

Plasmin is a serine protease generated through cleavage of the zymogen precursor plasminogen by plasminogen activator (tissue type or urokinase type, tPA or uPA). The precursor, plasminogen, a 92 kD protein, is primarily synthesized in the liver and circulates in the blood at 2-4 μ M (1). Several studies have explored plasminogen expression in the central nervous system (CNS, 2-4). For example, reverse transcription polymerase chain reaction and *in situ* hybridization studies have recently provided evidence for plasminogen mRNA in the cortex, hippocampus and cerebellum of both neonatal and adult mice (4). Similarly, tPA is known to be expressed in several brain regions, including the hippocampus, and is thought to be involved in learning as well as neuronal degeneration (2). Once tPA cleaves plasminogen, plasmin has numerous targets, the best known being fibrinogen. The fibrinolytic actions of plasmin mediate clot dissolution and thus play a critical role in blood hemostasis. Plasmin has also been shown to have functional effects in the brain, including cleavage of pro-brain-derived neurotrophic factor (pro-BDNF) to BDNF, which may play a critical role in the generation of long-term potentiation (LTP, 5). However, in addition to cleavage of fibrinogen and pro-BDNF, plasmin has also been reported to cleave a wide range of other substrates, including protease-activated receptors (PARs).

PARs are a class of receptors activated by proteolytic cleavage of the N-terminus by serine proteases. This cleavage reveals a new N-terminus that acts as a tethered ligand to activate the receptor. For example, activation of PAR1 by thrombin cleavage can initiate signaling through $G\alpha$ -i/o, $G\alpha$ -q/11, and $G\alpha$ -12/13 pathways (6-9). Plasmin can cleave PAR1 at Arg41 and PAR4 at Arg47 to activate these receptors (10). Additionally, plasmin cleaves

downstream of these activating sites on PAR1, as well as PAR2, subsequently terminating signaling by removing the tethered ligand (10, 11). As a result of the multiple plasmin cleavage sites in PAR1, plasmin-triggered PAR1 activation may have a different temporal signaling profile than thrombin-triggered PAR1 activation. In the CNS of both humans and rodents, PAR1 is widely expressed in astrocytes, while its neuronal expression appears to be more localized (6, 12, 13). In addition to plasmin, PAR1 can be activated by thrombin, Factor Xa, Factor VIIa, and small synthetic amino acid peptides that mimic the newly cleaved N-terminal (e.g. TFLLR, (14)). Activation of PAR1 by different proteases in different cells has been suggested to serve different functions, complicating the understanding of the potential actions of PAR1 (9).

The ability of plasmin to activate PAR1 suggests that brain-derived plasmin could influence normal CNS function. Therefore, it is important to more fully understand the role of PAR1 activation by plasmin in neuronal and glial physiology. Indeed, the tPA / plasminogen / plasmin system has previously been suggested to play important roles in normal brain function, including control of hippocampal neuronal plasticity, modification of the reward system, regulation of dopamine release from the nucleus accumbens, regulation of function within the bed nucleus of stria terminalis, as well as the CNS response to stress (5, 15-20). We have previously proposed that PAR1 activation triggers a complex cascade of events that culminates with potentiation of neuronal NMDA receptors (21-22). Interestingly, mice lacking PAR1 show deficits in forms of emotional memory (23) that depend on NMDA receptor function (24). Because NMDA receptors are Ca^{2+} permeable and are well-known to be involved in cellular processes underlying learning and memory (25-26), we hypothesize that the ability of plasmin to activate PAR1 and regulate NMDA receptor function could be linked to changes in learning and memory. In this report, we investigate the effects of plasmin on astrocytic and neuronal intracellular signaling as well as its effects on excitatory synaptic transmission in hippocampal slice preparations. Our findings suggest that plasmin can control synaptic NMDA receptor function through activation of astrocytic PAR1.

Experimental Procedures

Animals - *PAR1*^{-/-} and wild-type mice were created by breeding *PAR1*^{+/-} mice, a gift from Dr. Shaun Coughlin (University of California, San Francisco, CA, (27)), with C57BL/6 wild-type mice from Jackson Laboratory (Bar Harbor, ME). Heterozygous littermates were bred to generate littermate homozygous null mutants and wild-type controls that were > 99% C57BL/6, which were subsequently used to generate homozygous colonies. All procedures using animals were approved by the Emory University IACUC.

Neuronal and astrocytic cultures - Cultured astrocytes were prepared from P0-P3 postnatal mouse cortex. Cells were dissociated into a single-cell suspension by trituration through a Pasteur pipette and plated onto either 12 mm glass coverslips or 6-well plates coated with 0.05 mg/ml poly-D-lysine and grown in DMEM media (Gibco) supplemented with 25 mM glucose, 10% heat-inactivated horse serum, 10% heat-inactivated fetal bovine serum, 2 mM glutamine, 10 U/ml penicillin, and 10 µg/ml streptomycin.

Neuronal cultures were derived from E17 Sprague-Dawley rat pups. Briefly, cortical tissue was dissected, transferred into HBSS containing 5% penicillin/streptomycin and 10 µM HEPES, and incubated in trypsin containing 0.02% DNase at 37°C for 15 min. Tissue was then triturated and the supernatant resuspended in B27-supplemented Neurobasal media containing 2 mM L-glutamine and 5% fetal bovine serum. Cells were plated onto poly-D-lysine-coated coverslips and after three days received serum-free media.

All cultures were maintained at 37°C in a humidified 5% CO₂-containing atmosphere. As described previously, astrocyte cultures were ≥95% pure based on analysis of glial fibrillary acidic protein staining ((7), data not shown).

Measurement of phosphoinositide hydrolysis - Astrocyte cultures in 6-well plates were labeled overnight with 4 µCi/ml *myo*-[2-³H]inositol (20 Ci/mmol; American Radiolabeled Chemicals, Inc). Cells were then incubated for 20 min in DMEM buffered with 25 mM HEPES (pH 8.0) and 10 mM LiCl₂. Accumulation of radioactive inositol phosphates was measured following 60 min incubation with increasing concentrations of human plasmin (Haematologic Technologies). Unless specified otherwise, human plasmin was used in all subsequent experiments. After solubilization of

cells with 20 mM formic acid and neutralization with 0.7 M NH_4OH , [^3H]inositol monophosphate fractions were separated by anion exchange chromatography (AG 1-X8 Dowex, BioRad) using increasing amounts of ammonium formate. [^3H]inositol monophosphate content was assessed by liquid scintillation spectrometry. Measurements for each experiment were made in triplicate and averaged. The values reported were the mean of three separate experiments on cultures obtained from three different animals on three separate days.

Phospho-ERK1/2 Immunolabeling - Cultured mouse astrocytes or neurons were treated with 100 nM plasmin for 15 min at 37°C. Some cultures also received a 5 min pre-application of 1 μM BMS-200261 (Emory University Microchemical Facility) followed by co-application of 100 nM plasmin with 1 μM BMS-200261. Cells were then fixed in 4% paraformaldehyde at room temperature and washed in phosphate-buffered saline, 0.1% Triton-X and 3% bovine serum albumin in Tris-buffered saline (TBS). Cultures were incubated overnight at 4°C in monoclonal mouse antibody recognizing extracellular signal-regulated kinase phosphorylated at both threonine-202 and tyrosine-204 (phospho-ERK, 1:200, Cell Signaling, MA). After washing in TBS and incubating in rabbit anti-mouse IgG antibody conjugated to Texas Red (1:200, 4 h, Molecular Probes, CA), cells were mounted with Vectashield medium (Vector Laboratories, CA) and viewed with an Olympus IX71 microscope and Orca-ER cooled digital camera (Hamamatsu, NJ).

Western Blotting – Cultured wild-type or PAR1-/- astrocytes were treated with 100 nM plasmin, 30 μM TFLLR, or buffer for 15 min at 37°C and lysed. Cell lysates were sonicated, boiled in sample buffer, subjected to SDS-PAGE (13.5%) and transferred to nitrocellulose membranes (Bio-Rad). Membranes were then blocked with Tris-buffered saline containing 5% milk, 0.5% Tween 20, and 0.02% sodium azide for 1 h at room temperature and washed once in TBS supplemented with 0.1% Tween (TBS-T). Total ERK1/2 and phosphorylated ERK1/2 protein bands were detected by incubating membranes with total ERK1/2 antibody (1:300 in TBS-T) and phospho-ERK antibody (1:1,000 in TBS-T) overnight at 4°C. Membranes were then washed with TBS-T and incubated for 1 h with horseradish peroxidase-conjugated goat anti-rabbit IgG diluted 1:10,000 in TBS-T (Jackson ImmunoResearch Laboratories, Inc.).

The membranes were again washed and protein bands were detected by enhanced chemiluminescence. Densitometry to quantify protein expression levels was performed using Scion Image software (Scion Corporation) by measuring the integrated density of each protein band individually. Phospho-ERK1/2 levels were normalized to total-ERK1/2 levels for each treatment condition.

Whole cell patch clamp recording - Transverse rat hippocampal slices (300 μm) were obtained from 10-17 day old rats as previously described (28). Slices were placed in a recording chamber and superfused at 1.5 ml/min with artificial cerebrospinal fluid (ACSF) comprised of (in mM) 124 NaCl, 24 NaHCO_3 , 3.5 KCl, 1.5 CaCl_2 , 1.5 MgCl_2 , 1.25 NaH_2PO_4 , and 10 glucose saturated with 95:5% O_2/CO_2 . All recordings were performed at 23°C except recordings of EPSPs, which were performed at 34°C.

Spontaneous inhibitory postsynaptic currents (IPSCs) were recorded from CA1 pyramidal cells using visually guided whole-cell patch recordings in voltage clamp configuration. Thin-walled glass micropipettes were filled with (in mM) 140 KCl, 10 HEPES, 4 Mg-ATP, 0.3 $\text{Na}_3\text{-GTP}$, and 5 QX-314; pH was adjusted to 7.24 and osmolality to 310 mOsm. The ionotropic glutamate receptor antagonists D-2-amino-5-phosphonovalerate (D-APV, 50 μM) and 6-cyano-7-nitroquinoxaline-2,3-dione (CNQX, 25 μM) were included in the ACSF. Due to the high intracellular chloride concentration, IPSCs were inward currents at -60 mV. Both the frequency and peak amplitude of detected events were analyzed. The GABA_A receptor blocker bicuculline (10 μM) was added at the end of each experiment to verify that the spontaneous IPSCs were GABA_A receptor-mediated. Excitatory postsynaptic currents (EPSCs) were evoked using a bipolar stimulator and a stimulus of 10-100 μA (50 μs). Miniature EPSCs were recorded in the presence of 0.5 μM tetrodotoxin (TTX, Calbiochem, CA) and 10 μM bicuculline (Sigma, MO). Spontaneous IPSCs and miniature EPSCs were detected from a holding potential of -60 mV by using the Mini Analysis Program (Synaptosoft: www.synaptosoft.com). Evoked EPSPs were recorded under current clamp from CA1 pyramidal cells in response to Schaffer collateral stimulation as described above. The area was determined for each EPSP, and then a running average of nine consecutive EPSPs were determined. Because the time at which plasmin

reaches each cell will differ, the maximum potentiation by plasmin will occur at different times. We therefore analyzed the peak area for each cell from the running average, as described by Gingrich et al. (2000) (21). Peak area was normally distributed (Pearson test) and evaluated using a t-test.

Whole cell recordings of NMDA-evoked currents were obtained from CA1 pyramidal neurons in slices using 3-7 M Ω thin walled glass pipettes filled with a solution containing (in mM) 140 CsMeSO₄, 5 HEPES, 2 Mg-ATP, 0.03 Na-GTP, 5 phosphocreatine; pH was adjusted to 7.24 and osmolality to 310 mOsm. Whole cell NMDA receptor-mediated current responses in CA1 hippocampal pyramidal cells were evaluated in response to pulses of NMDA plus glycine (1 mM / 30 μ M) applied onto the dendrites using a pressurized micropipette. NMDA-evoked currents were measured every minute at a holding potential of -60 mV before and during the application of 100-200 nM plasmin (Haematologic Technologies) or 30 μ M TFLLR-NH₂ (hereafter TFLLR; Emory University Microchemical Facility). Changes in series resistance were monitored from the instantaneous current response to the -5 mV step and membrane resistance was estimated from the leak current. After five stable baseline measurements were taken, PAR1 agonist/antagonist or control solution was applied for 15-20 minutes.

Whole-cell patch clamp recordings (voltage clamp, holding at -60 mV) from 5- to 10-day cultured cortical neurons were made with an Axopatch 200B amplifier (Axon Instruments, Union City, CA) at room temperature (23°C). The recording chamber was continually perfused with recording solution composed of (in mM) 150 NaCl, 3 KCl, 2 CaCl₂, 5.5 glucose and 10 HEPES (pH 7.2 by NaOH; osmolality adjusted to 315 - 320 mOsm with sucrose) with or without 1.5 mM Mg²⁺. Thin wall glass pipettes were filled with (in mM): 110 D-Gluconate (50% w/w sol.), 110 CsOH (50% w/w sol.), 30 CsCl, 5 HEPES, 4 NaCl, 0.5 CaCl₂, 2 MgCl₂, 5 BAPTA, 2 NaATP, and 0.3 NaGTP (pH adjusted to 7.3 with CsOH and osmolality adjusted to 300-310 mOsm with sucrose). Drugs were applied directly by gravity and controlled by solenoid valves (Lee, Westbrook, CT). The pipette was placed above the recorded cell. Drug application had a relatively fast onset and achieved complete local perfusion of the recorded cell (full solution exchange within 100 msec). The peak and steady state amplitude of

NMDA-evoked current was measured in control and plasmin-treated groups (300 nM plasmin, 10 min, at 37°C). The Mg²⁺ sensitivity was evaluated by subtracting the responses to voltage ramps (-80 to +40 mV) before and during NMDA application in the presence of 1.5 mM Mg²⁺.

Two electrode voltage clamp recordings from Xenopus laevis oocytes - Stage V-VI oocytes from *Xenopus laevis* were isolated and injected with cRNA, as previously described (29). Briefly, mouse PAR1 and PAR2 were synthesized *in vitro* from cDNA according to manufacturer's specifications (Ambion, TX), and 2-10 ng of cRNA was injected. Mouse PAR1 and PAR2 cDNA were provided by Dr. Shaun Coughlin (UCSF). Mouse PAR3 and PAR4 RIKEN Mouse FANTOM™ cDNA clones were obtained from the Genome Exploration Research Group, RIKEN GSC, and a replica was provided by K.K. DNAFORM: FANTOM Consortium; RIKEN Genome Exploration Research Group and Genome Science Group (Genome Network Project Core Group, PAR3/4). Following 24-72 h after injection, oocytes were recorded from using two electrode voltage clamp (V_{HOLD} -40 mV). The recording solution contained (in mM) 60 NaCl, 40 KCl, 1.8 CaCl₂, 1 MgCl₂, and 6 HEPES; pH was adjusted to 7.4 with NaOH; recording electrodes contained 0.3 M KCl.

Activation of recombinant PAR in *Xenopus laevis* oocytes is known to increase intracellular Ca²⁺, which opens a calcium-activated chloride channel endogenously expressed in oocytes to produce an inward current response under voltage clamp (29-30). At -40 mV, all agonists for PAR1, PAR2, and PAR4 evoked an inward current in oocytes expressing recombinant PARs that was characteristic of the Ca²⁺-activated Cl⁻ current; this current was abolished in oocytes that were injected with 20 nl of 100 mM BAPTA to chelate intracellular calcium (n = 4-8 for each clone; data not shown). Oocytes that were not injected with any cRNA did not respond to TFLLR-NH₂ (hereafter TFLLR), 2f-LIGRLO, AYPGKF-NH₂ (hereafter AYPGKF) or thrombin (n = 6-20). Trypsin induced a small inward current responses in uninjected oocytes that was one-fifth of the amplitude of that observed in oocytes injected with mouse PAR2 mRNA (21% \pm 11; unpaired t-test; p < 0.01; n = 23). Mouse PAR3 did not produce detectable current responses to 10-50 nM thrombin.

To quantify PAR activation, a 2 min baseline perfusion with wash buffer was followed by application of peptide agonist or protease activator for 2 min. We measured the area under the curve. To evaluate the selectivity of BMS-200261 (synthesized by Emory University Microchemical Facility) for PAR1 blockade, 1 μ M BMS-200261 was pre-applied for 1 min followed by a 2 min co-application of 1 μ M BMS-200261 with peptide or protease agonist. Responses with and without BMS-200261 were run on the same day. The concentrations of thrombin and trypsin that were tested matched reported EC₅₀ values for mouse PAR1 and PAR2 (27, 31). Applying thrombin at the reported EC₅₀ concentration onto PAR4 (low nanomolar range) did not cause a current response in this system. We did see a reliable current response at 50 nM thrombin in oocytes injected with mouse PAR4 cRNA. We further evaluated the response to higher concentrations of thrombin to verify that 50 nM thrombin produced submaximal responses that were in the dynamic range of the concentration-effect curve. We similarly verified that concentrations of activators used for mouse PAR1 (1 nM thrombin) and mouse PAR2 (5 nM trypsin) were in the dynamic response range (n = 4-12 for PAR1, PAR2, PAR4).

Ca²⁺ imaging - Cultured astrocytes were incubated with 5 μ M Fura-2/AM or Fluo-3/AM in 1 μ M pluronic acid (Molecular Probes, CA) for 30 min at 37°C, and subsequently transferred to a microscope stage for imaging. External solution contained (in mM) 150 NaCl, 10 HEPES, 3 KCl, 2 CaCl₂, 2 MgCl₂, 5.5 glucose; pH was adjusted to 7.4 and osmolality to 325 mOsm. Following excitation at 340 nm and 380 nm, Fura-2 emission intensity at 510 nm was acquired as ratiometric images using an Olympus BX51WI microscope and a PTI IC200 intensified camera. Experiments with Fluo-3 used an excitation of 450-490 nm and band-passed emission (500-550 nm). Dose-response curves for plasmin were derived by using the FlexStation II plate reader (Molecular Devices, CA) to measure changes in Fluo-4 fluorescence in wild-type mouse astrocytes plated onto 96-well plates. Fluo4/AM dye loading and agonist application were performed according to manufacturer instructions.

Electrodes for simultaneous whole cell patch recording and Ca²⁺ imaging were filled with (in mM) 140 potassium gluconate, 10 HEPES, 7 NaCl, 4 Mg-ATP, 0.3 Na₃-GTP, 0.1 Fluo-3 or Oregon Green; pH was adjusted to

7.24 and osmolality to 310 mOsm. To eliminate synaptic activity, 1 μ M TTX was added to the oxygenated ACSF. Throughout the experiments -5 mV voltage steps of 15 ms duration were applied at 30 sec intervals from a holding potential of -70 mV to continuously monitor the holding current, series resistance, and membrane input resistance. After entering whole cell mode, cells were maintained for ~20 min to allow filling with Fluo-3 before image acquisition. After the baseline period, plasmin (200 nM) was applied and images were acquired every 5-10 s with 25-50 ms exposure to 450-490 nm light. Fluorescence was recorded through a band-passed filter (500-550 nm) using a Princeton Micromax camera. Fluorescence intensity was measured in cell bodies using Imaging Workbench 2.2.1 (INDEC BioSystems, CA) and expressed as F/F₀ where F₀ is the fluorescence intensity prior to drug treatment. For all experiments, increases in fluorescence greater than 1.2-fold were considered to be relevant changes. Baseline fluorescence values possessed a peak F/F₀ ratio of 1.01 \pm 0.01 during a typical experiment. Peak F/F₀ ratio was used to measure the effect of plasmin over control.

RESULTS

Plasmin activation of PAR1 signaling in astrocytes. Plasmin has previously been shown to stimulate inositol triphosphate (IP3) production in hippocampal slices through PAR1 activation (32). We measured the ability of plasmin to stimulate IP3 formation in purified astrocyte cultures, and found that plasmin induced PI hydrolysis with a half-maximal activating concentration (EC₅₀) of approximately 64 nM (n = 3 separate experiments, Fig. 1A). Because IP3 production triggers an increase in intracellular Ca²⁺ concentration ([Ca²⁺]_i) by mobilizing calcium from IP3-sensitive intracellular stores, we subsequently tested whether plasmin also increases [Ca²⁺]_i in cultured astrocytes. Indeed, plasmin caused an increase in [Ca²⁺]_i in purified wild-type astrocytic cultures (mean \pm sem 195 \pm 6.7 % increase over baseline, n = 4; Fig. 1B-D). Both human and mouse plasmin were able to increase [Ca²⁺]_i in mouse astrocytes with EC₅₀ values of 65 nM and 120 nM, respectively (n = 4 separate experiments, Fig. 1C). Although cultured PAR1-/- astrocytes still showed measurable phosphoinositide accumulation following a one hour exposure to plasmin (n = 3, data not shown), they exhibited significantly lower peak

$[Ca^{2+}]_i$ increase than wild-type astrocytes ($141 \pm 6.2\%$ peak over baseline, $p < 0.001$, $n = 9$ experiments; Fig. 1D).

While plasmin can cleave PAR1, it has been suggested to be less potent and less efficacious than thrombin (10-11). Previous reports have also suggested that plasmin may cleave other targets, including PAR4 and laminin (33, 34), although some data supporting this idea is indirect. To further test whether the plasmin-mediated increase in astrocytic $[Ca^{2+}]_i$ might reflect activation of PAR1, we tested the sensitivity of astrocytic plasmin response to the competitive PAR1 antagonist BMS-200261 (35). Both TFLLR- and plasmin-triggered mobilization of $[Ca^{2+}]_i$ was blocked by 1 μ M BMS-200261 (Fig. 2A-B, $p < 0.001$, $n = 5$ separate experiments). The ability of 100 nM plasmin to increase astrocytic $[Ca^{2+}]_i$ was also blocked by the plasmin antagonist α_2 -antiplasmin (200 nM, $n = 4$), but not by the thrombin antagonist hirudin (30 ATU; $n = 4$ experiments; Fig. 2C), a dose that effectively inhibits thrombin signaling through PAR1 (data not shown, $n=4$ experiments). In addition, inhibition of the catalytic domain of plasmin using a serine protease inhibitor, (4-amidinophenyl)-methane-sulfonyl fluoride (100 μ M), also significantly blocked the ability of plasmin to trigger release of intracellular Ca^{2+} in astrocytes (data not shown, $n = 3$ experiments; $p < 0.05$). These data together suggest that catalytic activity of plasmin on PAR1, rather than other contaminant proteases such as thrombin, trigger the increase in astrocytic $[Ca^{2+}]_i$.

To evaluate the specificity of the PAR1 antagonist BMS-200261, we used two electrode voltage clamp recordings from *Xenopus* oocytes injected with cRNA encoding mouse PARs. To quantify PAR1, PAR2, and PAR4 receptor activation, we measured inward currents generated by Ca^{2+} -activated Cl^- channels (see *Methods*). Treatment of PAR3 cRNA-injected oocytes with thrombin did not induce any consistent current response in oocytes. We found that 1 μ M BMS-200261 blocked mouse PAR1 activation by the selective peptide agonist TFLLR both at maximally effective (30 μ M, $p = 0.02$; Table 1) and half-maximally effective concentrations (5 μ M, $p < 0.01$, Table 1). However, there was no effect of BMS-2000261 on activation of PAR2 by the peptide agonist 2-furoyl-LIGRLO (20 μ M or 2 μ M, $p > 0.05$), or on activation of murine PAR4 by the selective peptide AYPGKF (50 or 500 μ M, $p > 0.05$; see

Table 1). Similar data were obtained using BMS-200261 to block submaximal concentrations of activating proteases for PAR1 (thrombin), PAR2 (trypsin), and PAR4 (thrombin; Table 1). These data indicate that 1 μ M BMS-200261 selectively inhibits PAR1 among the protease receptor family in an oocyte expression system. Thus, our experiments showing BMS-200261 block of plasmin signaling in astrocytes further suggest that plasmin activates PAR1-linked calcium signaling in astrocytes. The observation that astrocytes isolated from PAR1^{-/-} animals retain some capacity to increase intracellular calcium and phosphoinositide hydrolysis in response to plasmin (Fig. 1D and data not shown) differs from results obtained in slices (32), and suggests that plasmin may also signal through another as yet unrecognized receptor expressed in cultured astrocytes.

PAR1 activators, such as thrombin and TFLLR, are known to activate p44/42 mitogen-activated protein kinase (MAPK, or ERK1/2) in astrocytes (7, 8). In order to examine whether plasmin has a similar effect, we treated isolated mouse astrocytes and neurons with 100 nM plasmin for 15 minutes with or without 1 μ M BMS-200261. After fixation, cells were immunolabeled with a monoclonal antibody targeting the dually phosphorylated ERK1/2. Plasmin-treated astrocytes exhibited markedly increased levels of peri-nuclear and nuclear phospho-ERK1/2 immunolabeling ($n = 3$ separate experiments; Fig. 3A). Application of 1 μ M BMS-200261 inhibited this plasmin-induced effect in astrocytes ($n = 3$; Fig. 3B). Moreover, western blot analyses of phosphorylated ERK1/2 levels in wild-type and PAR1^{-/-} astrocytes further demonstrate that plasmin triggers astrocytic ERK1/2 activation at least partly through PAR1 (Fig. 3C).

In contrast, plasmin did not trigger detectable changes in neuronal phospho-ERK1/2 immunolabeling ($n = 2$ experiments; data not shown), suggesting that plasmin primarily affects ERK1/2 signaling in astrocytes. Furthermore, while plasmin (200 nM) increased astrocytic $[Ca^{2+}]_i$ in primary hippocampal cultures, it had no effect on somatic Fluo-3 fluorescence in neurons, suggesting that plasmin has no effect on neuronal $[Ca^{2+}]_i$ (Fig. 4A; 1.06 ± 0.02 fold increase over baseline, $n = 4$). Similarly, 200 nM plasmin did not markedly alter Fluo-3 or Oregon Green fluorescence in CA1 pyramidal cells in acute slices (Fig. 4C; 1.08 ± 0.01 fold increase over baseline, $n = 3$ cells

from 3 different slices). These data indicate that plasmin can elevate intracellular Ca^{2+} and trigger ERK1/2 phosphorylation in astrocytes more readily than in hippocampal neurons.

These results suggest that our previous study (21) overestimated the degree to which PAR1 activation triggers intraneuronal Ca^{2+} signaling (we reported that 40% of cultured hippocampal neurons showed a response). As discussed in Lee et al. (22), this overestimation likely resulted from imaging mixed hippocampal and dentate neurons and glial cells. In those experiments, insufficient resolution between different cell types, as well as higher PAR1 expression in the dentate, likely led to this overestimate. Our subsequent studies in hippocampal slices and acutely dissociated cells (22), as well as other reports (36), suggest a lower percentage of hippocampal neurons (4-10%) respond to PAR1 activation with increases in intracellular Ca^{2+} . This is also consistent with immunostaining in brain tissue, which shows more prominent astrocytic than neuronal expression of PAR1 (6).

Plasmin effects on synaptic signaling. The plasmin-induced increase in astrocytic $[\text{Ca}^{2+}]_i$ suggests a potentially active role for this molecule in modulating synaptic transmission through active and reciprocal cross-talk between astrocytes and neurons (37). Astrocytic glutamate has recently been shown to modulate extrasynaptic NMDA receptors (38), inhibitory neurotransmission (39) and AMPA receptor-mediated neurotransmission (40) in CA1 pyramidal cells. We therefore studied whether the plasmin-induced astrocyte signaling described above is able to modulate inhibitory and excitatory neurotransmission in CA1 pyramidal neurons.

We first recorded spontaneous inhibitory postsynaptic currents (IPSCs) in CA1 pyramidal cells from hippocampal slices before and during application of 200 nM plasmin. Experiments were performed in the presence of a competitive NMDA receptor antagonist (D-APV, 50 μM) and a competitive AMPA/kainate receptor antagonist (CNQX, 25 μM) to both isolate IPSCs and rule out indirect effects on IPSC properties from any potential astrocytic release of glutamate. Neither the frequency nor the amplitude of spontaneous IPSCs was affected by up to a 6 minute application of 200 nM plasmin (Fig. 5), a level previously shown to activate PAR1 in hippocampal slices (32). Spontaneous IPSC frequency was not significantly different between control (7.4 ± 1.6 Hz) and plasmin

application (7.1 ± 1.4 Hz; $n=7$ cells from 7 different slices; $p>0.05$; Fig. 5B). Similarly, plasmin had no effect on the cumulative probability distributions of spontaneous IPSC inter-event intervals (Fig. 5D, left panel). Plasmin (200 nM) did not significantly alter the mean spontaneous IPSC amplitude (control: 51 ± 10 pA vs. plasmin: 53 ± 12 pA, $n=7$; $p>0.05$; Fig. 5C) or the cumulative distribution of spontaneous IPSC amplitudes (Fig. 5D, right panel). These data suggest that plasmin does not directly modulate recurrent GABAergic neurotransmission in CA1 pyramidal cells. These results are in contrast to a previous report in which 100 nM plasmin modestly decreased GABA_A receptor-mediated currents (41).

We subsequently evaluated the effect of plasmin on excitatory synaptic transmission. Spontaneous EPSCs were relatively infrequent in CA1 pyramidal cells, leading us to study EPSCs evoked by Schaffer collateral stimulation. We pharmacologically isolated AMPA receptor-mediated EPSCs by recording in the presence of 50 μM D-APV and 10 μM bicuculline (see *Methods*). Plasmin (200 nM) did not significantly alter evoked EPSC amplitude (control $102 \pm 3.8\%$ vs. plasmin $107 \pm 3\%$; $n=5$ cells; $p > 0.05$; Fig. 5E), suggesting that plasmin-mediated activation of astrocytic PAR1 did not influence AMPA receptor-mediated excitatory neurotransmission. These findings are consistent with previously reported data showing that plasmin did not influence AMPA receptor-mediated synaptic transmission (41).

Activation of PAR1 by thrombin has previously been shown to potentiate NMDA receptor function (21). Although plasmin has been reported to have no effects on NMDA receptor responses, these experiments were done in the absence of Mg^{2+} , which is required for PAR1's actions on NMDA receptors (21). In order to explore the effects of plasmin on synaptic NMDA receptors under normal ionic conditions, we recorded spontaneous miniature excitatory postsynaptic currents (mEPSCs) in CA1 pyramidal cells held under voltage clamp at -60 mV in the presence 1.5 mM extracellular Mg^{2+} and 0.5 μM TTX. We evaluated the amplitude, frequency, and decay kinetics of mEPSCs, which can be described by a single fast decay due to voltage-dependent block of the slow synaptic NMDA receptor component by extracellular Mg^{2+} . As previously shown, mEPSCs (frequency 0.1-0.5 Hz) recorded in the presence of 10 μM bicuculline (filtered at 1 kHz;

-3dB) could be divided into subgroups based on their rise time (22). We used this approach to distinguish fast rising mEPSCs (rise time less than 5 ms) from slow rising mEPSCs (rise time between 5 and 10 ms; Fig. 6A). We assume that this broad distribution of rise times reflects different electrotonic distances from the somatic recording site of synapses giving rise to mEPSCs (42-44). Application of 200 nM plasmin prolonged the decay of the slow rising mEPSCs compared to control without significantly changing either the peak amplitude or the mEPSC frequency (Fig 6C). The prolonged time course reflected the appearance of a second slow decay time constant in the presence of plasmin that was characteristic of NMDA receptor-mediated component of EPSCs (Fig 6C). This plasmin-dependent uncovering of the slow component of the mEPSC decay was sensitive to the competitive NMDA receptor blocker D-APV (50 μ M), whereas average peak amplitude of the fast AMPA receptor component (control 14.3 ± 1.2 pA, plasmin 12.9 ± 0.9 pA, $p > 0.05$) and frequency of mEPSCs (control 0.11 ± 0.02 Hz, plasmin 0.14 ± 0.03 Hz, $p > 0.05$) were unaffected by D-APV (Fig. 6BC).

The NMDA-component of the mEPSC persisted in normal (1.5 mM) Mg^{2+} , suggesting that either Mg^{2+} sensitivity had been reduced or that the holding potential of the distal dendrites had been compromised. The increase in decay was only observed in the mEPSCs with a slower rise time (>5ms), which we interpret to represent quantal events arising at distal synapses under modest voltage control. No effect was observed in the mEPSCs with faster rise time (<5 ms), assumed to arise from more proximal and well voltage-clamped synapses.

In order to evaluate the effect of plasmin on excitatory synaptic transmission that involves both AMPA and NMDA receptors, we stimulated the Schaffer collateral to evoke EPSPs from CA1 pyramidal cells under current clamp in the presence of 1.5 mM extracellular Mg^{2+} . We found that addition of 200 nM plasmin significantly enhanced the area of the EPSP response by 1.20 ± 0.07 fold (t-test, $p < 0.02$; $n = 11$ cells from 11 slices). Figure 7AB shows plasmin-induced potentiation of the evoked EPSP waveform and EPSP area in a representative cell. Interestingly, not all cells responded to plasmin (Fig 7C), similar to the results obtained with thrombin (21). These data further suggest that plasmin can potentiate the NMDA receptor component of synaptic transmission.

In order to reliably evaluate NMDA receptor response amplitude following plasmin application, we used pressure application of NMDA and glycine in stratum radiatum of CA1 in hippocampal slices and recorded the whole cell current response under voltage clamp (Fig. 8A). This paradigm ensures that the amount of NMDA receptor agonist is constant throughout the experiment. Experiments were performed in the presence of 0.5 μ M TTX and 10 μ M bicuculline to eliminate effects of IPSCs and spontaneous synaptic currents (see *Methods*). All experiments were concluded by verifying that currents studied were sensitive to D-APV. Using this approach, we found that plasmin, as well as TFLLR, strongly potentiated the peak amplitude of the NMDA-induced current (Fig. 8B-D). Furthermore, both TFLLR- and plasmin-mediated potentiation of NMDA receptor-mediated currents was inhibited by co-application of the selective PAR1 antagonist BMS-200261 (1 μ M; Fig. 8B-D), suggesting that the primary effect of plasmin on NMDA receptor responses involved activation of PAR1 rather than effects of plasmin binding or catalysis on substrates other than PAR1.

Interestingly, plasmin did not potentiate the NMDA receptor current in isolated cultured cortical neurons without astrocytes present either in the absence or presence of extracellular Mg^{2+} (Fig. 9). Plasmin had no effect on NMDA response waveform. Similar results were found in the presence of 3 μ M ifenprodil to isolate non-NR2B containing NMDA receptors (data not shown). In addition, plasmin did not alter the sensitivity to Mg^{2+} in isolated neurons (Fig. 9CD). These data support our working hypothesis that plasmin activation of PAR1 indirectly potentiates the NMDA response in slices through relief of Mg^{2+} block, rather than directly through modification of NMDA receptor function or the inherent Mg^{2+} sensitivity of the receptor. This result is consistent with a large number of experiments with PAR1 activators in cultured neurons, acutely dissociated neurons, and mammalian HEK-293 cells transfected with PAR1 and NMDA receptor subunits (22). However, this result is in contrast to previously reported potentiation by PAR1 co-expressed in oocytes with NMDA receptor subunits (21). Given that both data sets are reliable and reproducible, our conclusion is that PAR1 engages second messenger systems in oocytes that are not operational in mammalian cells. This conclusion raises a significant caveat regarding

the use of heterologous expression systems to study post-translational receptor regulation.

DISCUSSION

The most important finding of this study is that plasmin is able to activate astrocytic PAR1 and potentiate neuronal NMDA receptor function in tissue but not in isolated neurons. This is the first characterization of the functional effects of plasmin in astrocytes. Inhibition of PAR1 blocks plasmin-induced signaling in astrocytes as well as plasmin-mediated potentiation of NMDA receptor function. These results suggest a role of astrocytic PAR1 in plasmin potentiation of neuronal NMDA receptor function in the presence of Mg^{2+} . These data also raise the possibility that tPA cleavage of brain-derived plasminogen to form plasmin may represent an activating system for PAR1 that can control excitatory synaptic transmission. Consistent with this idea, tPA can stimulate IP3 formation in hippocampal slices, and this effect is blocked in plasminogen knockout mice and in PAR1 knockout mice (32).

Role of tPA/plasmin-PAR1 signaling in the CNS. The effects of plasmin-triggered PAR1 activation on the NMDA receptor-mediated component of excitatory synaptic transmission described here are consistent with previously described effects of the tPA/plasmin system in brain tissue. Specifically, the expression of tPA has been shown to increase during activity-dependent forms of synaptic plasticity, and inhibition or removal of tPA blocks the late phase of LTP induced by either forskolin or tetanic stimulation in the hippocampal mossy fiber and Schaffer collateral pathways (45-47). Since LTP is NMDA receptor-dependent, it seems likely that tPA generation of plasmin may enhance NMDA receptor responsiveness, thereby altering the mechanisms underlying LTP formation. Plasmin itself has also been suggested to control synaptic plasticity. Plasmin can enhance short term plasticity in hippocampal slices, whereas the plasmin inhibitor α 2-antiplasmin can attenuate LTP (47). Plasmin also appears to control plasticity in the nucleus accumbens, again an NMDA receptor-dependent process (15). Moreover, the tPA/plasmin system regulates reverse occlusion-induced neuronal plasticity within the visual cortex (48). Chronic inhibition of either tPA or plasmin in the visual cortex prevents both morphological and functional neuronal recovery following eye reopening (48). While the mechanisms remain

unknown, together these studies suggest that under normal conditions the endogenous tPA/plasmin cascade facilitates neuronal restructuring and synaptic efficacy throughout the CNS. In this report, we propose a downstream signaling mechanism by which tPA/plasmin may promote synaptic plasticity, in part through plasmin-mediated PAR1 activation on astrocytes with consequent potentiation of NMDA receptor-driven neuronal responses. In support of the proposed PAR1 involvement in neuronal plasticity, PAR1^{-/-} animals show deficits in two forms of emotional learning that are known to be NMDA receptor-dependent (23).

Plasmin potentiation of NMDA receptor function. Immunohistochemical studies have shown that PAR1 protein is expressed mainly in human astrocytes of white and gray matter in the cortex, hippocampus, caudate, putamen, and cerebellum (6). By contrast, larger pyramidal neurons of the hippocampus and cortex show only modest PAR1 immunoreactivity in human brain (6). Similarly, in the rat brain PAR1, PAR2, PAR3, and PAR4 are functionally co-expressed in cultured astrocytes (13). Consistent with these findings, we observe strong functional PAR1 expression in astrocytes, but not in neurons in rat hippocampal slices or in isolated cultured mouse neurons. Furthermore, plasmin does not potentiate NMDA receptor responses in isolated neurons cultured in the absence of astrocytes, but does potentiate NMDA receptor responses in tissue in the presence of Mg^{2+} . Interestingly, plasmin has been reported to have no effect on NMDA receptor function in the absence of Mg^{2+} (47), suggesting that depolarization-induced relief of Mg^{2+} blockade may be required for plasmin-induced potentiation. Together, these data lead us to hypothesize that plasmin may control neuronal transmission through cross-talk between astrocytes and neurons. Interestingly, PAR1 activation can generate lysophosphatidic acid and arachidonic acid in platelets and endothelial cells, respectively (49-50). Both of these lipid signaling molecules are highly mobile and capable of mediating inter-cellular signaling. Although it is not yet known whether astrocytic PAR1 activation can trigger formation of these lipids, release of lysophosphatidic acid or arachidonic acid could potentially play a role in the effects described here. Whereas arachidonic acid can directly potentiate neuronal NMDA receptor function (51), lysophosphatidic acid has been suggested to enhance NMDA receptor

function through depolarization-induced relief of Mg^{2+} block (52).

Recent observations support the possibility that astrocytes can regulate excitatory and inhibitory neuronal transmission (38-40, 47). We have recently shown that application of TFLLR, a selective PAR1 agonist, onto wild-type astrocytes co-cultured with PAR1^{-/-} neurons will produce NMDA-mediated Ca^{2+} and current responses in neurons (22). These neuronal effects are not observed in the presence of PAR1^{-/-} astrocytes, suggesting that PAR1 activation triggers astrocytes to release a molecule, such as glutamate, that signals to neurons. Indeed, depolarization of astrocytes has been shown to cause release of glutamate and most likely other neuroactive factors (53). Furthermore, this astrocyte-derived signal has been suggested to potentiate synaptic NMDA

receptor responses through relief of voltage-dependent Mg^{2+} blockade at dendritic spines. We interpret the current results as showing that plasmin-mediated potentiation of NMDA receptor function in brain tissue is PAR1-dependent and suggest that plasmin engages this previously described astrocyte-neuronal cross-talk (22).

In conclusion, these data together suggest that plasmin can activate PAR1 in astrocytes and consequently trigger astrocyte-mediated NMDA current potentiation in CA1 pyramidal cells. Our results suggest a possible role of this serine protease in regulating excitatory synaptic transmission under normal conditions, and from these data we predict that plasmin may have a role in controlling synaptic function and plasticity.

REFERENCES

- Zhang, L., Seiffert, T., Fowler, B.J., Jenkins, J.R., Thinnes, T.C., Loskutoff, D.J., Parmer, R.J., Miles, L.A. (2002) *Thromb Haemost* **87**, 493-501
- Melchor, J.P., Strickland, S. (2005) *Thromb Haemost* **93**, 655-660
- Salles, F.J., Strickland, S. (2002) *J Neurosci* **22**, 2125-2134
- Basham, M.E., Seeds, N.V. (2001) *J Neurochem* **77**, 318-325
- Pang, P.T., Teng, H.K., Zaitsev, E., Woo, N.T., Sakata, K., Zhen, S., Teng, K.K., Yung, W.H., Hempstead, B.L., Lu, B. (2004) *Science* **306**, 487-491
- Junge, C., Lee, C.J., Hubbard, K.B., Zhang, Z., Olson, J.J., Hepler, J.R., Brat, D.J., Traynelis, S.F. (2004) *Exp Neurol* **188**, 94-103
- Nicole, O., Goldshmidt, A., Hamill, C.E., Sorensen, S.D., Sastre, A., Lyuboslavsky, P., Hepler, J.R., McKeon, R.J., Traynelis, S.F. (2005) *J Neurosci* **25**, 4319-29
- Sorensen, S.D., Nicole, O., Peavy, R.D., Montoya, L.M., Lee, C.J., Murphy, T.J., Traynelis, S.F., Hepler, J.R. (2003) *Mol Pharmacol* **64**, 1199-1209
- Traynelis SF, Trejo J (2007) *Curr Opin Hematol* **14**, 230-235.
- Kuliopulos, A., Covic, L., Seeley, S.K., Sheridan, P.J., Helin, J., Costello, C.E. (1999) *Biochemistry* **38**, 4572-4585
- Loew, D., Perrault, C., Morales, M., Moog, S., Ravanat, C., Schuhler, S., Arcone, P., Pietropaolo, C., Cazenave, J.P., van Dorsselaer, A., Lanza, F. (2000) *Biochemistry* **39**, 10812-10822
- Niclou, S.P., Suidan, H.S., Pavlik, A., Vejsada, R., Monard, D. (1998) *Eur J Neurosci* **10**, 1590-1607
- Wang, H., Ubl, J.J., Reiser, G. (2002) *Glia* **37**, 53-63
- Hollenberg, M.D., Saiffedine, M., al-Ani, B., Kawabata, A. (1997) *Can J Physiol Pharmacol* **75**, 832-841.
- Nagai, T., Yamada, K., Yoshimura, M., Ishikawa, K., Miyamoto, Y., Hashimoto, K., Noda, Y., Nitta, A., Nabshima, T. (2004) *Proc Natl Acad Sci USA* **101**, 3650-3655
- Pawlak, R., Nagai, N., Urano, T., Napiorkowska-Pawlak, D., Ihara, H., Takada, Y., Collen, D., Takada, A. (2002) *Neurosci* **113**, 995-1001.
- Pawlak, R., Rao, B.S., Melchor, J.P., Chattarji, S., McEwen, B., Strickland, S. (2005) *Proc. Natl. Acad. Sci. USA* **102**: 18201-18206.
- Matys T., Pawlak R., Strickland S. (2005) *Neurosci* **135**: 715-22.
- Ito M., Nagai H., Kamei H., Nakamichi N., Nabeshima T., Takuma K., and Yamada K. (2006) *Mol Pharmacol* **70**, 1720-1725.

20. Nagai, T. Ito, M., Nakamichi, N., Mizoguchi, H., Kamei, H., Fukakusa, A., Nabeshima, T., Takuma, K., and Yamada, K. (2006) *J Neurosci* **26**, 12374-12383.
21. Gingrich, M.B., Junge, C., Lyuboslavsky, P., and Traynelis, S. (2000) *J Neurosci* **20**, 4582-4595.
22. Lee, J.C., Mannaioni, G., Yuan, H., Woo, D.H., Gingrich, M.B., and Traynelis, S.F. (2007). *J Physiol* **581**, 1057-1081.
23. Almonte A.G., Hamill C.E., Chhatwal J.P., Wingo T.S., Barber J.A., Lyuboslavsky P.N., Ressler K.J., Holtzman S.G., White D.A., Traynelis S.F. (2007) *Neurobiol Learn Mem* **88**, 295-304.
24. Walker, D.L., Davis, M. (2002) *Pharmacol Biochem Behav* **71**, 379-92.
25. Lisman J. (2003) *Philos. Trans. R. Soc. Lond. B. Biol. Sci.* **358**, 829-842.
26. Nicoll R.A. (2003) *Philos. Trans. R. Soc. Lond. B. Biol. Sci.* **358**, 721-726.
27. Connolly, A.J., Ishihara, H., Kahn, M.L., Farese, R.V. Jr., Coughlin, S.R. (1996) *Nature* **381**, 516-519
28. Mannaioni, G., Marino, M.J., Valenti, O., Traynelis, S.F., Conn, P.J. (2001) *J Neurosci* **21**, 5925-5934
29. Dascal, N., and Cohen, S. (1987) *Pflügers Arch* **409**, 512-520
30. Oron, Y., Dascal, N., Nadler, E., Lupu, M. (1985) *Nature* **313**, 141-143
31. Mari B, Guerin S, Far DF, Breitmayer JP, Belhacene N, Peyron JF, Rossi B, Auberger P. (1996) *FASEB J* **10**:309-16
32. Junge, C.E., Sugawara, T., Mannaioni, G., Alagarsamy, S., Conn, P.J., Brat, D.J., Chan, P.H., Traynelis, S.F. (2003) *Proc Natl Acad Sci USA* **100**, 13019-13024
33. Chen, Z.L., Strickland, S. (1997) *Cell* **91**, 917-925
34. Quinton, T.M., Kim, S., Derian, C.K., Jin, J., Kunapuli, S.P. (2004) *J Biol Chem* **279**, 18434-18439
35. Bernatowicz, M.S., Klimas, C.E., Hartl, K.S., Peluso, M., Allegretto, N.J., Seiler, S.M. (1996) *J Med Chem* **39**, 4879-4887
36. Yang Y., Akiyama H., Fenton J.W. 2nd, Brewer G.J. (1997) *Brain Res* **761**, 11-18
37. Carmignoto, G. (2000) *Prog Neurobiol* **62**, 561-581
38. Fellin, T., Pascual, O., Gobbo, S., Pozzan, T., Haydon, P.G., Carmignoto, G. (2004) *Neuron* **43**, 729-743
39. Kang, J., Jiang, L., Goldman, S.A., Nedergaard, M. (1998) *Nat Neurosci* **1**, 683-692
40. Fiacco, T.A., McCarthy, K.D. (2004) *J Neurosci* **24**, 722-732
41. Mizutani, A., Tanaka, T., Saito, H., Matsuki, N. (1997) *Brain Res* **761**, 93-96
42. Rall, W. (1962) *Biophys J* **2**, 145-167
43. Smith, M.A., Ellis-Davies, G.C., Magee, J.C. (2003) *J Physiol* **548**, 245-258
44. Stricker, C., Field, A.C., Redman, S.J. (1996) *J Physiol* **490**, 419-441
45. Baranes, D., Lederfein, D., Huang, Y.Y., Chen, M., Bailey, C.H., Kandel, E.R. (1998) *Neuron* **21**, 813-825
46. Huang, Y.Y., Bach, M.E., Lipp, H.P., Zhuo, M., Wolfer, D.P., Hawkins, R.D., Schoonjans, L., Kandel, E.R., Godfraind, J.M., Mulligan, R., Collen, D., Carmeliet, P. (1996) *Proc Natl Acad Sci USA* **93**, 8699-8704
47. Mizutani, A., Saito, H., Matsuki, N. (1996) *Brain Res* **739**, 276-81
48. Muller, C.M., Griesinger, C.B. (1998) *Nature Neurosci* **1**, 47-53
49. Eichholtz, T., Jalink, K., Fahrenfort, I., Moolenaar, W.H. (1993) *Biochem J* **291**, 677-680.
50. Rickard, A., Portell, C., Kell, P.J., Vinson, S.M., McHowat, J. (2005) *Am J Physiol Renal Physiol* **288**, F714-F721.
51. Miller, B., Sarantis, M., Traynelis, S.F., Attwell, D. (1992) *Nature* **355**, 722-725.
52. Holtsberg, F.W., Steiner, M.R., Furukawa, K., Keller, J.N., Mattson, M.P., Steiner, S.M. (1997) *J Neurochem* **69**, 68-75.
53. Nedergaard, M., Takano, T., and Hansen, A.J. (2002) *Nat Rev Neurosci* **3**, 748-755.

FOOTNOTES

* We thank Jan Pohl for synthesizing TFLLR-NH₂, AYPGKF-NH₂, and BMS-200261. We also thank Antoine Almonte, Phuong Le, Kimberly Haustein and Rohini Polavarapu for excellent technical

assistance, and Shaun Coughlin for generously providing PAR1 +/- animals as well as cDNA for mouse and human PAR receptors. This work was supported by NINDS (SFT, MY), NARSAD (SFT, GM), NIH NRSA fellowship support (AGO, CEH, CJL), and the Ente Cassa di Risparmio di Firenze, Italy (GM).

¹The abbreviations used are: tPA, tissue-type plasminogen activator; uPA, urokinase-type plasminogen activator; CNS, central nervous system; BDNF, brain-derived neurotrophic factor; LTP, long-term potentiation; PAR, protease-activated receptor; TTX, tetrodotoxin; ACSF, artificial cerebrospinal fluid; TBS, tris-buffered saline; phospho-ERK, phosphorylated extracellular signal-regulated kinase; IPSCs, inhibitory postsynaptic currents; EPSCs, excitatory postsynaptic currents; IP3, inositol triphosphate; EC₅₀, half-maximal activating concentration; [Ca²⁺]_i, intracellular calcium concentration; MAPK, mitogen-activated protein kinase; mEPSCs, miniature excitatory postsynaptic currents.

FIGURE LEGENDS

Fig. 1. Plasmin increases intracellular Ca²⁺ ([Ca²⁺]_i) in cultured astrocytes. *A*, Dose-response curve obtained from plasmin-induced IP3 release in cultured mouse astrocytes; expressed as percentage of baseline hydrolysis (n = 3 separate experiments). *B*, Ratiometric images (340 nm/380 nm excitation, 510 nm emission) of Fura-2/AM-loaded cultured mouse astrocytes during baseline and 100 nM plasmin application. Color scale shows the pseudocolor coding of ratio values ranging from low to high (ratio values 1 to 3). *C*, Increase in Fluo-4 fluorescence induced by application of the indicated concentrations of either human-derived plasmin (*left panel*) or mouse-derived plasmin (*middle panel*) in mouse astrocytes. Response to 30 μM TFLLR is also shown. Average baseline Fluo-4 fluorescence within each well was used to calculate percent change in fluorescence during agonist application (*arrowhead*). Each trace is an average of 4 trials in one experiment using the indicated dose and agonist. (*C, right panel*) Dose-response curve for human- and mouse-derived plasmin using Fluo-4 imaging in cultured mouse astrocytes (n = 4 experiments). *D*, During perfusion of wild-type or PAR1^{-/-} astrocytes loaded with Fura-2/AM with buffer or 100 nM plasmin (60 s, *arrowhead*), ratiometric imaging was conducted by alternating between 340 nm and 380 nm excitation and acquiring at 540 nm emission. Each blue trace shows the ratio of one astrocyte during the course of a recording from one coverslip. Mean traces are shown in red. Representative of ≥ 4 experiments performed with different cultures prepared on different days. (*D, bar graph*) Peak plasmin responses are lower in PAR1^{-/-} astrocytes as compared to wild-type astrocytes (n ≥ 4 separate experiments, # p < 0.001, Student's t-test). Average peak response to 100 nM plasmin application in wild-type and PAR1^{-/-} cultured astrocytes (baseline recorded for ≥ 30 s).

Fig. 2. Plasmin increases [Ca²⁺]_i in cultured cortical astrocytes through activation of PAR1. *A, top panel*, Time-course of astrocytic calcium responses to 300 nM plasmin (30 s application, *left*), 30 μM TFLLR (10 s application, *middle*), and 10 μM 2-methylthio-ATP (2-MT-ATP, 10 s application, *right*). Each blue trace shows the ratio of one cultured astrocyte during the course of a recording from a coverslip with multiple cells. Mean traces ± s.e.m. from an experiment are shown in red. *A, bottom panel*, Time course of plasmin, TFLLR, and 2-methylthio-ATP responses in the presence of BMS-200261 (1 μM), a PAR1 antagonist. *B-C*, The percentage of wild-type astrocytes exhibiting > 20% increase above baseline in Fura-2/AM ratio in response to 100 nM plasmin was significantly decreased by both 1 μM BMS-200261 (from 56% to 4%; # p < 0.001, n = 5 separate experiments performed with different cultures prepared on different days) and by 200 nM α₂-antiplasmin (*C, left panel*, from 56% to 19%; # p < 0.001, n = 4 separate experiments). *C, right panel*, Hirudin (30 anti-thrombin units or ATU), a thrombin inhibitor, had no effect on plasmin responses.

Fig. 3. Plasmin activates ERK1/2 in cultured astrocytes. *A*, Untreated (control) astrocytes exhibited low-to-moderate levels of phospho-ERK1/2 immunolabeling in the cytoplasm, while astrocytes treated with 100 nM plasmin for 15 minutes showed intense peri-nuclear and nuclear labeling (arrows); scale bar = 50 μm. *B*, PAR1 antagonist BMS-200261 (BMS, 1 μM) inhibited plasmin-induced increase in nuclear phospho-ERK1/2 immunolabeling in astrocytes, while exposure

to the antagonist alone had no effect. Images are representative of 3 separate experiments performed with different cultures prepared on different days. Between 2-4 coverslips were tested in each experiment per trial. *C*, Representative Western blot showing increased phospho-ERK levels in astrocytes treated with either TFLLR (30 μ M) or plasmin (100 nM) for 15 min. Quantification of western blot analysis is shown at right. Two-way ANOVA found main effects of both agonist and genotype ($p < 0.05$, $F = 4.1$ and 6.74 for agonist and genotype, respectively), with plasmin inducing a significant response in WT astrocytes (vs. baseline; $*p < 0.05$). Values were normalized to total ERK levels and baseline ($n = 6$ separate experiments performed on cultures prepared on different days).

Fig. 4. Plasmin increases $[Ca^{2+}]_i$ in astrocytes from primary hippocampal cultures with no effect on $[Ca^{2+}]_i$ in neurons from primary hippocampal cultures or hippocampal slices. *A*, Plasmin (200 nM) stimulates an increase in somatic Fluo-3 fluorescence in cultured hippocampal astrocytes (*arrow*), with no significant effect on neurons (*asterisk*). Fluorescence is shown in dark on this reverse image. Neurons were identified by the presence of a response to NMDA (50 μ M) application, which triggered a strong increase in somatic Fluo-3 fluorescence (*not shown*). *B*, *left panel*, Time course of the effect of plasmin (200 nM) on Fluo-3 fluorescence in a single astrocyte and neuron shown in *panel A*. *B*, *right panel*, bar graph expressing the peak ratio of Fluo-3 fluorescence induced by plasmin (mean \pm s.e.m.; $n = 4-6$ separate experiments). *C*, Images are shown from a single CA1 pyramidal neuron loaded through a patch clamp pipette with the membrane impermeable dye Fluo-3 during buffer, plasmin (200 nM), and (1S,3R)-1-aminocyclopentane-1,3-dicarboxylic acid (ACPD, 100 μ M) application. Fluorescence is shown in dark on this reverse image. The time-course of Ca^{2+} fluorescence for this cell is shown below. Data are representative of recordings from 3 cells in 3 different slices made from 2 animals on two different days.

Fig. 5. Plasmin does not alter spontaneous IPSCs or evoked AMPA-receptor-mediated EPSCs. Plasmin application does not affect the frequency (panels *A-B*) or the amplitude (*C-D*) of pharmacologically isolated spontaneous IPSCs in CA1 hippocampal neurons. *E*, Plasmin does not modulate the AMPA receptor mediated component of the evoked EPSC (eEPSC) amplitude (evoked by electrical stimulation of the Schaffer-CA1 synapse in CA1 hippocampal neurons).

Fig. 6. Plasmin potentiates the NMDA receptor component of mEPSCs in the presence of extracellular Mg^{2+} . *A*, The frequency histogram of 180 mEPSCs recorded from 5 cells (each from a different slice) for a time period of 5 min each shows the rise time variability of mEPSCs. Experiments were performed on slices prepared from two different mice on two different days. Panels *B* and *C* show the superimposed scaled average traces and fitted exponential decay time courses of fast and slow rise time mEPSCs both in control (*red*) and in the presence of plasmin 200 nM (*green*). The curves were fitted with a single exponential component. The scaled average traces and fitted decay curves of the slow rise mEPSCs show a second, slower exponential component only in the presence of plasmin (*green*) compared to control (*red*), which we interpret to reflect the uncovering of an NMDA receptor-mediated component. The competitive NMDA receptor antagonist D-APV blocked the plasmin-induced slow exponential component. Right panels show average time constant for fast rising mEPSCs fitted to a single exponential component (*panel B*), or the mEPSC time course fitted to a dual exponential component fit (*panel C*) with a fast (*open bar*) and slow (*filled bar*) component. When no filled bar is shown, the second slower component could not be detected.

Fig 7: Plasmin potentiates the NMDA receptor component of evoked EPSPs in the presence of extracellular Mg^{2+} . *A*, The *left panel* shows the average EPSP waveform prior to addition of plasmin. Superimposed (in gray) is the response recorded at the end of the experiment in the presence of D-APV. The right panel shows the EPSP waveform after addition of plasmin, superimposed on the response in the presence of D-APV. Assuming the AMPA receptor component of the EPSP is insensitive to plasmin, as suggested by our data (Fig 5E), the difference between the waveforms in the presence and absence of D-APV represents the NMDA contribution to the EPSP. *B*, The average time course of the area of the EPSP from a representative cell; each symbol represents the average of three responses. *C*, The average peak response was determined as described in the *Methods*; individual peak responses from 11 cells are shown as superimposed symbols ($p < 0.01$, t-test).

Fig. 8. Plasmin potentiates NMDA receptor current responses in CA1 pyramidal cells in the presence of 1.5 mM extracellular Mg^{2+} . *A*, Schematic illustration of whole cell patch recording arrangement in rat hippocampal slices. Current responses of CA1 pyramidal cells to pressure-ejected NMDA (1 mM) were recorded under voltage clamp (V_{HOLD} -60 mV) before and during application of either 100 nM plasmin or 30 μ M TFLLR (see *Methods*). *B*, Plasmin potentiated the response amplitude of NMDA receptor currents. The effect of plasmin was blocked by the selective PAR1 antagonist BMS-200261 (1 μ M). Peak fold potentiation was obtained by normalizing the responses to baseline recordings prior to drug application, and calculating the running average of three sequential responses throughout the response time course. Also shown is the response in control cells treated with ACSF alone. The number of cells is shown in parentheses. *C-D*, Average peak potentiation in control and TFLLR- or plasmin-treated cells was taken as the maximum of the running average of consecutive response amplitudes (* $p < 0.05$, Kruskal-Wallis and Dunn post-hoc test).

Fig. 9. Plasmin treatment has no effect on the amplitude or Mg^{2+} sensitivity of NMDA-evoked whole-cell currents in isolated cultured cortical neurons. *A*, The peak and steady-state amplitude of agonist-evoked whole cell currents (50 μ M NMDA/glycine; V_{HOLD} -60 mV) were 1005 ± 126 pA and 369 ± 37 pA in control group ($n = 7$), 1188 ± 168 pA and 401 ± 70 pA ($n = 6$) in the plasmin-treated group (300 nM, 10 min), with no significant difference between groups ($p = 0.40$ for peak amplitude, $p = 0.68$ for steady-state amplitude, Student's t-test). *B*, Summary of peak and steady-state amplitude of NMDA-evoked currents in control and plasmin-treated groups; similar results were found when 3 μ M ifenprodil was added to remove the contribution of NR2B-containing receptors (data not shown, $n = 13-14$). *C*, Superimposed I-V curves show that plasmin treatment has no effect on the Mg^{2+} sensitivity. I-V curves for NMDA-evoked currents were obtained by subtracting the responses to voltage ramps (-80 to +40 mV) before and during NMDA application in the presence of 1.5 mM Mg^{2+} . The currents were normalized to that measured at +40 mV, and the membrane potential was corrected for the junction potential (+10 mV (21)). Note that the I-V curve of plasmin-treated group (black line) was nearly superimposable with the control group (gray line). *D*, Summary of ratio of NMDA-evoked current at +30 mV and -30 mV relative to the reversal potential in control and plasmin-treated groups. There is no significant difference between groups (control: 4.25 ± 0.25 ; plasmin: 4.44 ± 0.15 ; $p = 0.54$; Student's t-test).

Table 1: BMS-200261 selectively blocks PAR1 signaling

	EC ₅₀ conc. of peptide (control, %)	EC ₅₀ conc. of peptide (+BMS, %)	Maximal conc. of peptide (control, %)	Maximal conc. of peptide (+BMS, %)	EC ₅₀ conc. of protease (control, %)	EC ₅₀ conc. of protease (+BMS, %)
mPAR1	100±33 (13)	7±11 (12) *	100±17 (23)	40±11 (18) *	100±21 (9)	47±10 (10) *
mPAR2	100±46 (13)	114±49 (17)	100±30 (21)	95±41 (17)	100±32 (13)	136±27 (11)
mPAR4	100±21 (26)	82±11 (18)	100±20 (14)	88±16 (12)	100±25 (29)	120±35 (28)

Oocytes expressing each protease receptor were challenged with their selective peptide activator at either EC₅₀ or maximal concentration. For mouse PAR1, the peptide agonist TFLLR was administered at 5 or 30 μM. For mouse PAR2, the peptide agonist 2f-LIGRLO was administered at 2 or 20 μM. For mouse PAR4, the peptide agonist AYPGKF was administered at 50 or 500 μM. The integral of the responses over 1 min was measured, averaged across all oocytes, and set to 100 ± s.e.m. %. A separate set of oocytes were pre-exposed to 1 μM BMS-200261 for 1 min and then challenged with agonist in the presence of BMS-200261. Responses were expressed as percent of mean control. We also tested the ability of BMS-200261 to block PARs that were activated by serine proteases. EC₅₀ values of activating proteases were used, which were 1 nM thrombin (PAR1), 5 nM trypsin (PAR2), and 50 nM thrombin (PAR4). These concentrations were confirmed to give submaximal responses (data not shown). Uninjected oocytes did not respond to peptide or thrombin application, but gave responses to trypsin that were 20% of those observed in PAR2 cRNA injected oocytes (see *Methods*). Number of oocytes are given in parentheses (*p < 0.05).

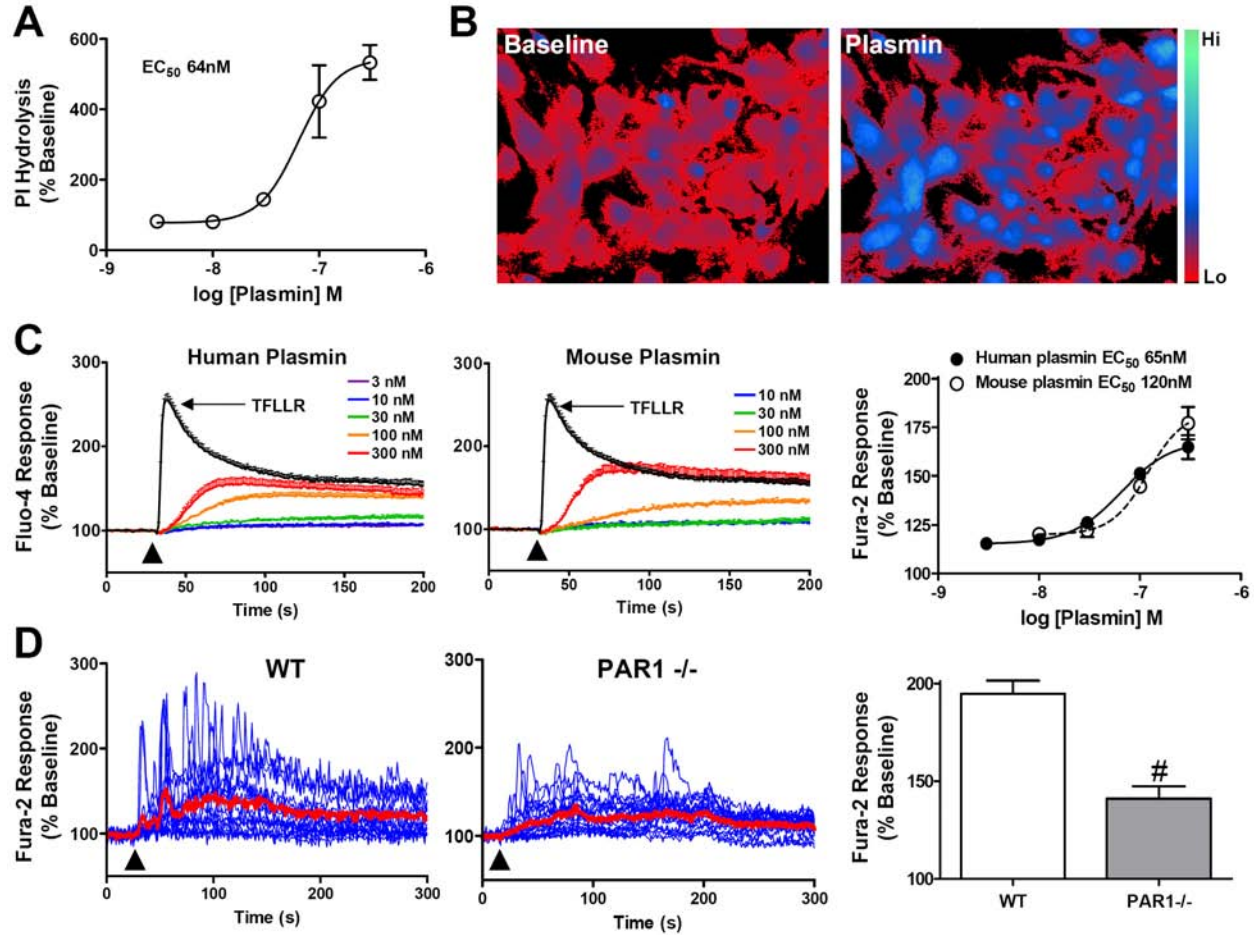


Figure 1

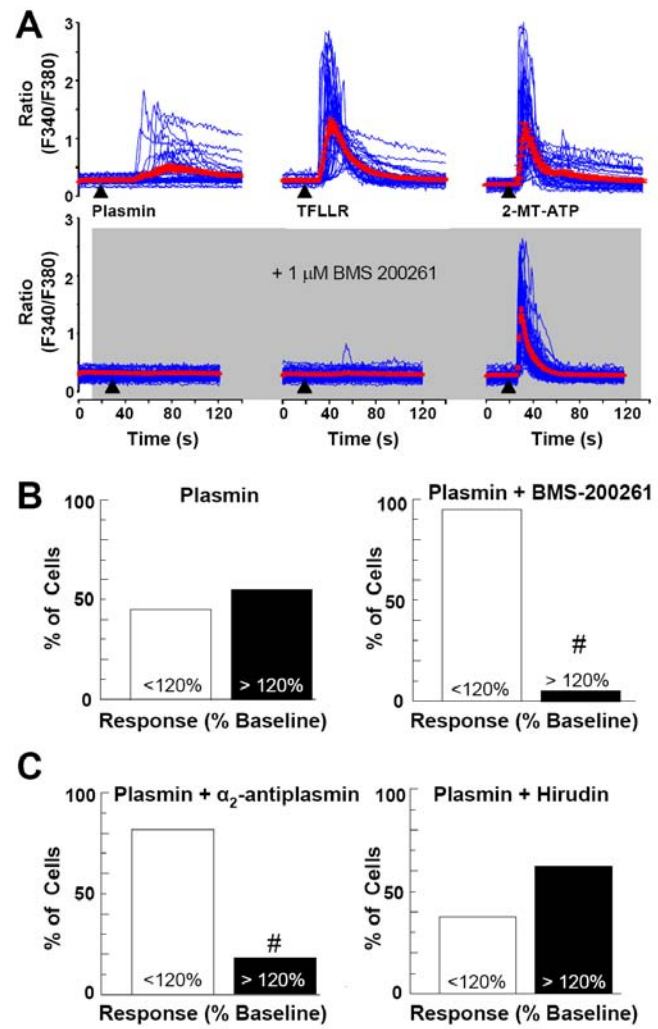


Figure 2

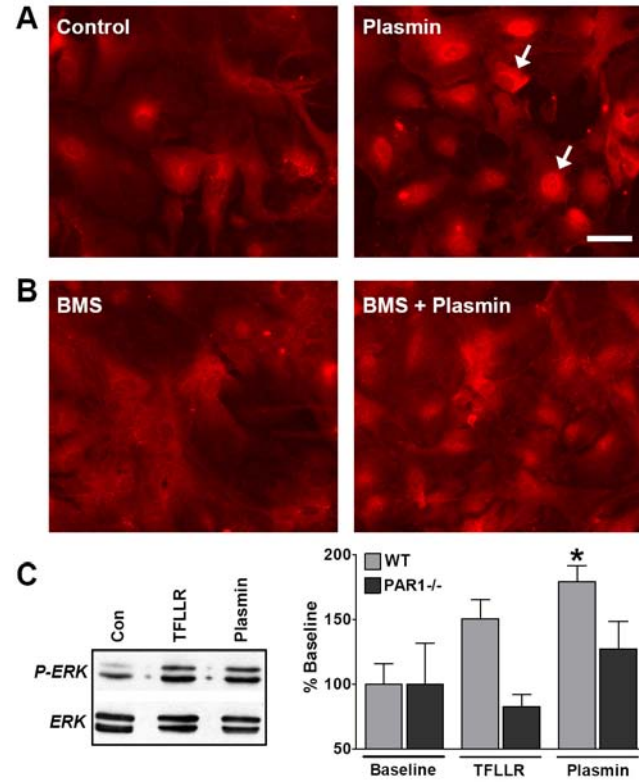


Figure 3

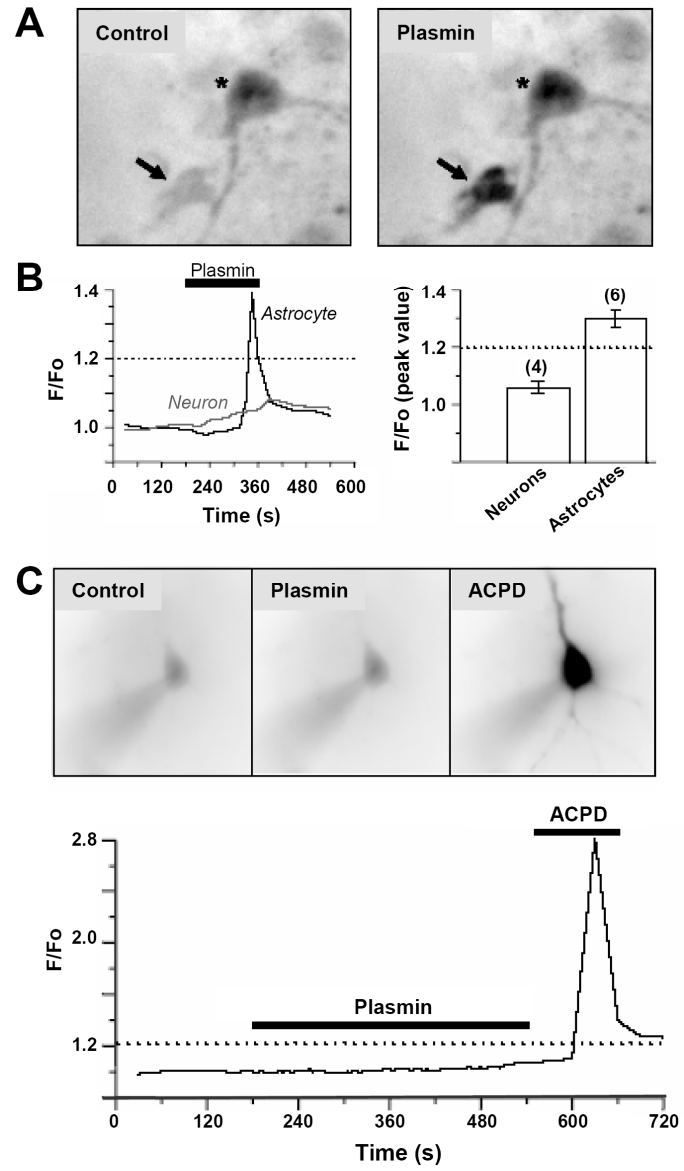


Figure 4

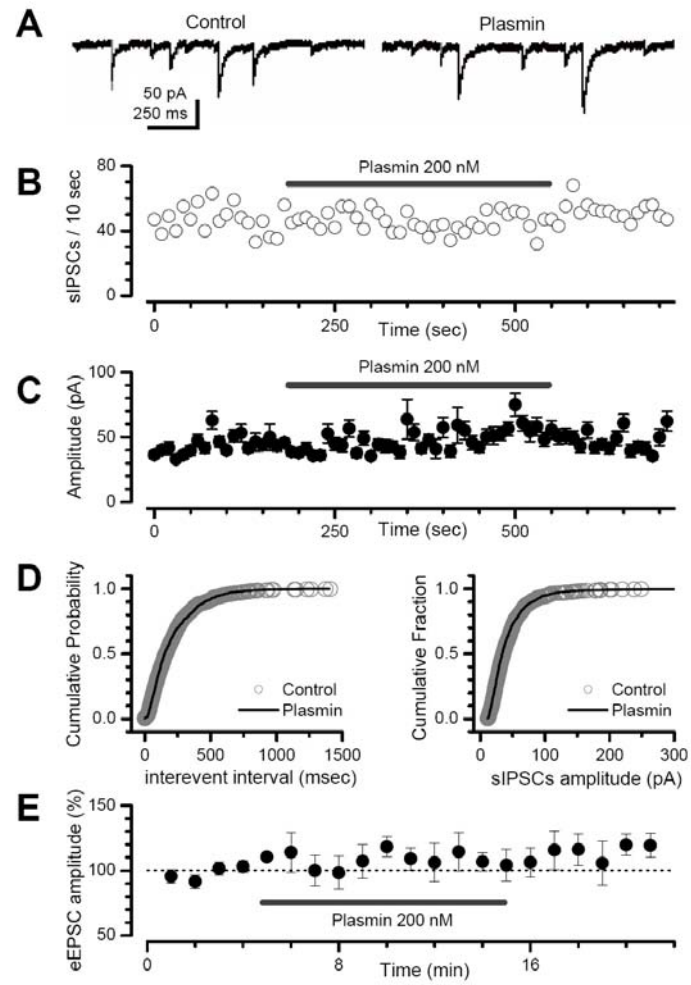
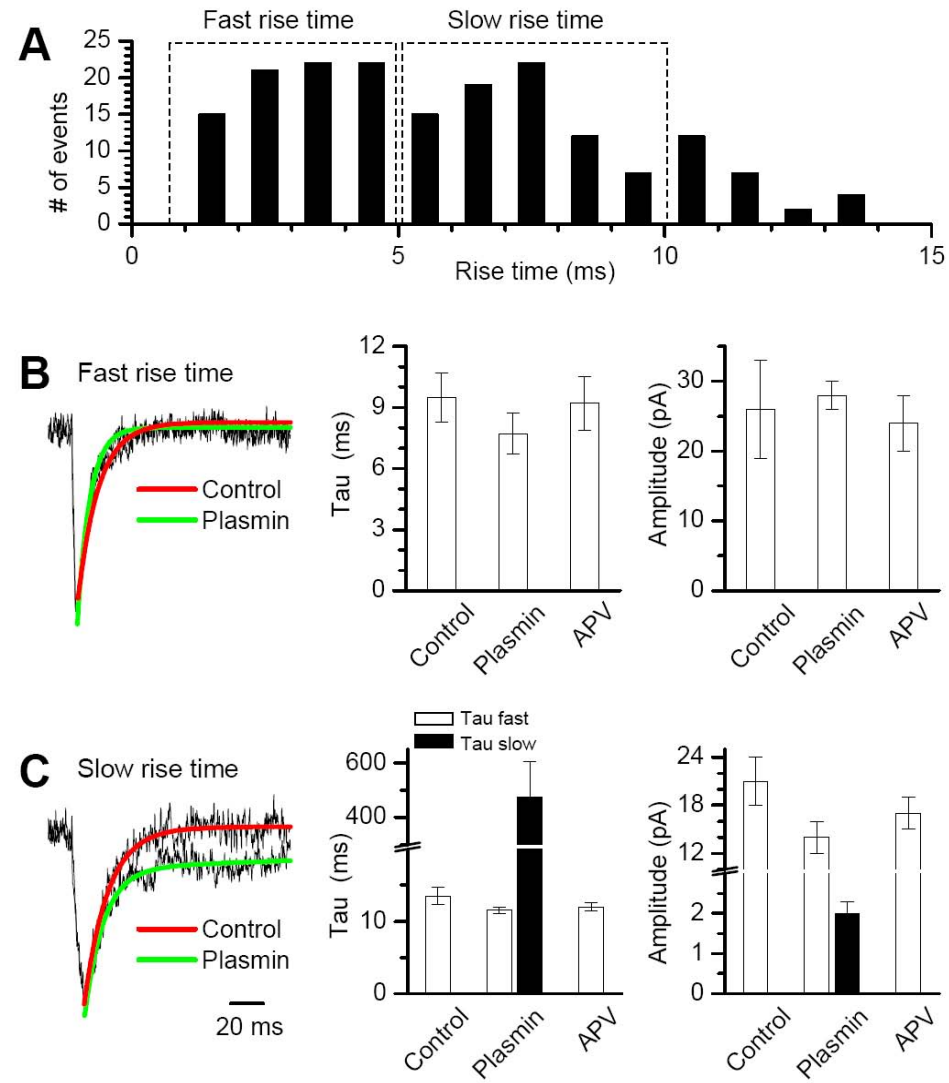


Figure 5



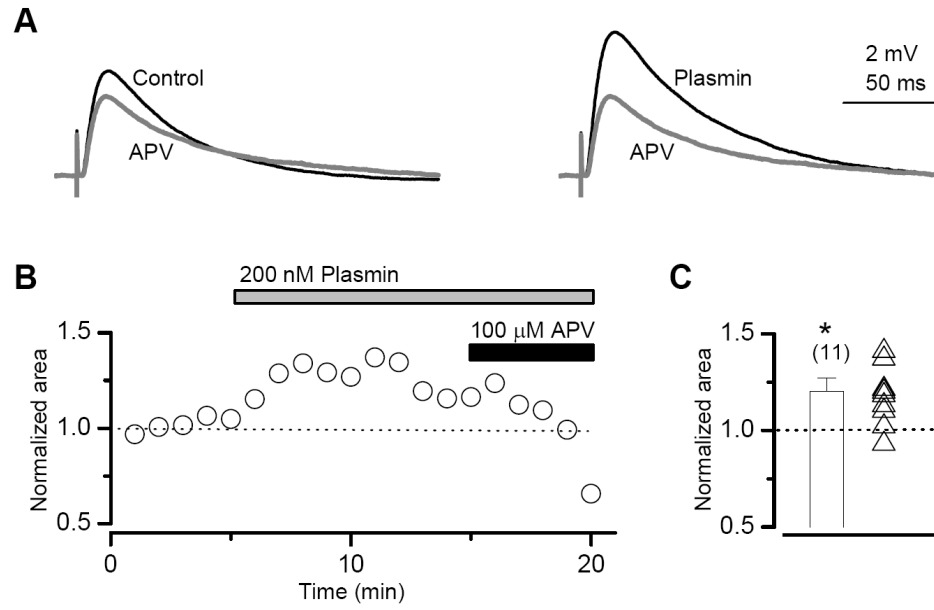


Figure 7

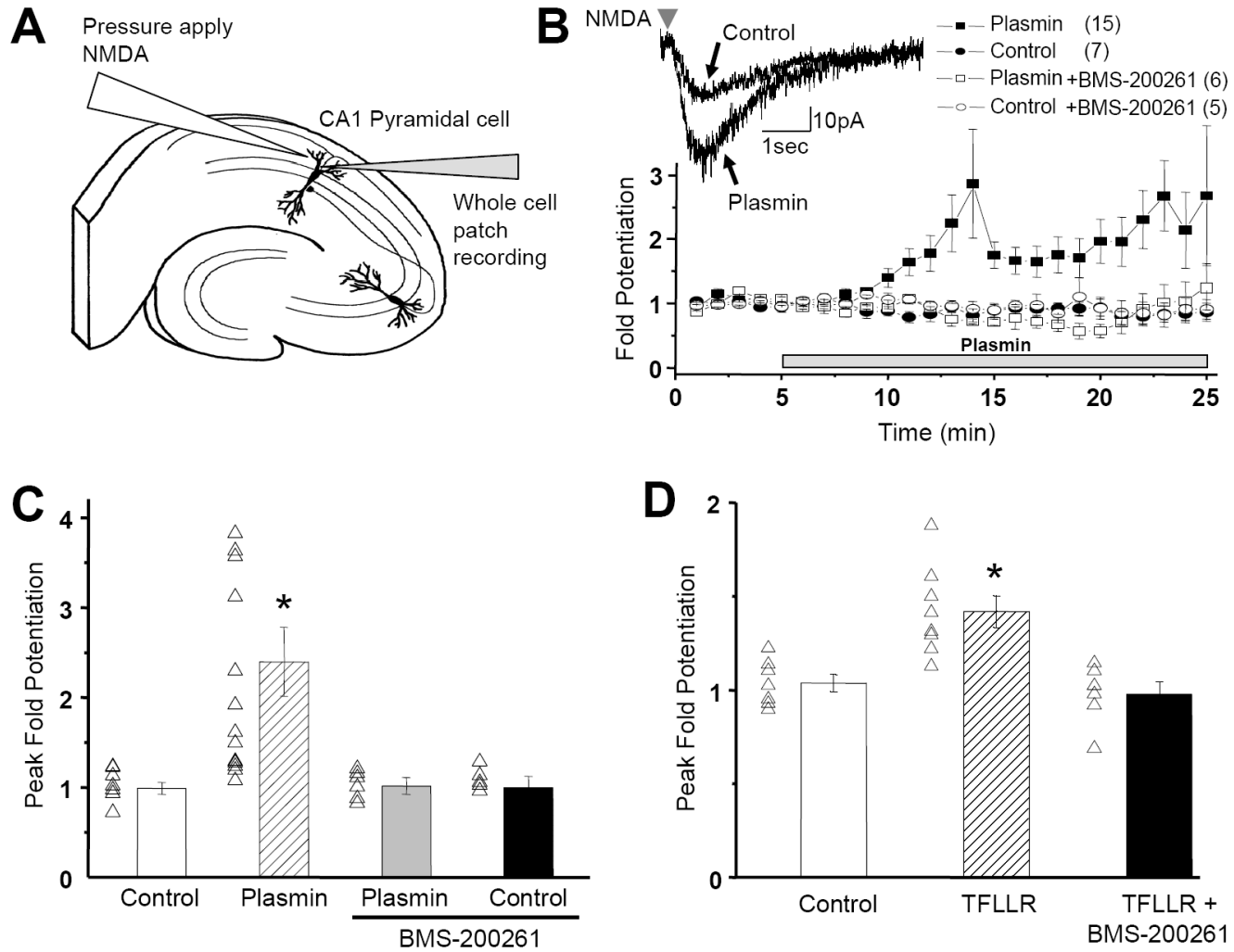


Figure 8

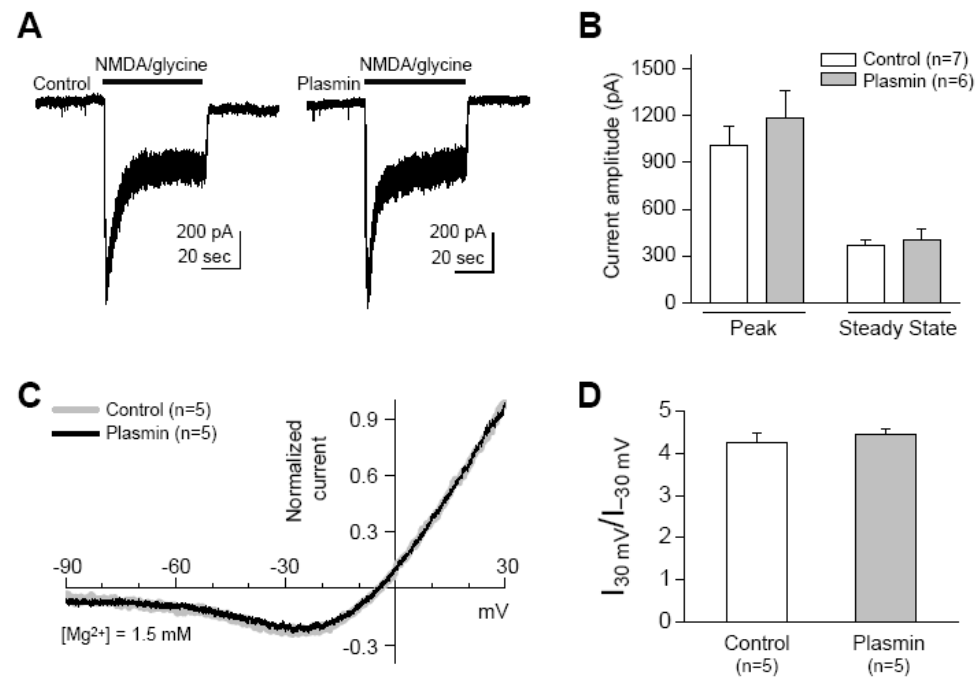


Figure 9